Vol. 31, 1980, pp. 523-530.

[7]Leibovich, S., and Stewartson, K., "A Sufficient Condition for the Instability of Columnar Vortices," *Journal of Fluid Mechanics,* Vol. 126, 1983, pp. 335-356.

[8]Stewartson, K., and Capell, K., "On the Stability of Ring Modes in a Trailing Line Vortex: the Upper Neutral Points," *Journal of Fluid Mechanics,* Vol. 156, 1985, pp. 369-386.

[9]Duck, P., "The Inviscid Stability of Swirling Flows: Large Wavenumber Disturbances," *Journal of Applied Mathematics and Physics,* Vol. 37, May 1986, pp. 340-360.

[10]Saric, W. S., and Nayfey, A. H., "Nonparallel Stability of Boundary-Layer Flows," *Physics of Fluids,* Vol. 8, Aug. 1975, pp. 945-950.

[11]Bertolotti, F. P., "Compressible Boundary Layer Stability Analyzed With the PSE Equations," AIAA 22nd Fluid Dynamics, Plasma Dynamics and Lasers Conference, AIAA Paper 91-1637, Honolulu, HI, June 1991.

[12]Hall, M. G., "Vortex Breakdown," *Annual Review of Fluid Mechanics,* Vol. 4, 1972, pp. 195-218.

[13]Hall, M. G., "A Numerical Method for Solving the Equations for a Vortex Core," Royal Aircraft Establishment, Tech. Rept. No. 65106, Farnborough, England, UK, May 1965.

[14]Batchelor, G. K., and Gill, A. E., "Analysis of the Stability of Axisymmetric Jets," *Journal of Fluid Mechanics,* Vol. 14, 1962, pp. 529-551.

[15]Malik, M. R., and Orszag, S. A., "Efficient Computation of the Stability of Three-Dimensional Compressible Boundary Layers," AIAA 14th Fluid and Plasma Dynamics Conference, AIAA Paper 81-1277, Palo Alto, CA, June 1981.

# Characterization of Droplet/Vapor/ Vortex Interactions in a Two-Dimensional Shear Layer

R. D. Hancock*
*U.S. Air Force Wright Laboratory,*
*Wright-Patterson Air Force Base, Ohio 45433*
and
L. P. Chin†
*Systems Research Laboratories, Inc., Dayton, Ohio 45440*

## Introduction

TWO-PHASE flows are often difficult to characterize because of the complex interaction of the solid particles or liquid droplets and the gas. These flows become even more complicated when the fundamental characteristics of the particles or droplets change due to such processes as evaporation and combustion. These complex flows are commonplace in such devices as industrial burners, internal-combustion engines, and gas turbine combustors. In many cases, the droplet or particle sizes and velocities can be measured, and the gas velocity can also be determined using a variety of velocimetry techniques. However, little information is available on the vapor after it leaves the surface of the evaporating droplet.[1-4] This information is particularly important in combusting sprays because combustion typically takes place away from the surface of the droplet where the fuel-to-air ratio is appropriate.

The visualization technique presented in this Note is a new method for accurate visualization and prediction of the convective transport of vapor in two-phase flows. Water droplets are injected into a $TiCl_4$-laden gaseous flow where they evaporate. The water vapor reacts spontaneously with the $TiCl_4$ vapor to form micrometer-sized $TiO_2$ particles. The particles are sufficiently small to accelerate rapidly to the velocity of the carrier gas but are too large to diffuse readily. Thus, they are convected along the path that the water vapor follows as it leaves the droplets. The instantaneous locus of the $TiO_2$ particles is defined as a "vaporline" and can be visualized using Mie scattering. Although the technique for visualizing vaporlines is relatively simple, the physics required to interpret the vaporlines in terms of the droplet, vapor, and fluid interactions can be complicated. The goal of this study was to provide insight into the physics needed to understand and interpret vaporlines. Additionally, predictions from a computer model are presented that support the qualitative interpretation of the vaporline data.

Presented as Paper 93-0416 at the AIAA 31st Aerospace Sciences Meeting, Reno, NV, Jan. 11-14, 1993; received Feb. 10, 1993; revision received July 20, 1993; accepted for publication July 26, 1993.

*Captain, Wright Laboratory, WL/POSF Bldg. 490, 1790 Loop Road N. Member AIAA.

†Senior Research Engineer, 2800 Indian Ripple Road. Member AIAA.

## Experimental

The experimental data presented in this Note were obtained in the two-dimensional shear-layer facility described in more detail elsewhere.[5] The splitter plate divides a 12.7-cm-square duct equally. Dry air was used in both airstreams. The gas velocities were set at 0.70 m/s and 0.35 m/s for the high- and low-speed sides of the flow giving localized Reynolds numbers of less than 1000. The higher-speed air was passed over a liquid $TiCl_4$ bath for collection of $TiCl_4$ vapor, as is done in reactive Mie scattering (rms).[6] For rms, two gaseous flows—one seeded with water vapor, the other with $TiCl_4$ vapor—must come in molecular contact. When the $TiCl_4$ reacts with the water vapor, $TiO_2$ particles are formed that act as light scatterers to mark the interaction of the two streams. The products of the $TiCl_4$ and $H_2O$ reaction are HCl and $TiO_2$. The $TiO_2$ is a fine white powder that is quite inert, but the HCl can create problems because of its corrosive nature. The quantity of HCl produced is quite low, but a hood should always be used when trying to visualize a flow with $TiCl_4$.

Droplets were injected through a slot in the Plexiglas duct on the low-speed side of the flow. The droplets were ~60 μm in diameter and had sufficient momentum to cross the shear layer to the high-speed, $TiCl_4$-laden side of the flow. Micrometer-sized $TiO_2$ particles were formed as the water vapor mixed with the $TiCl_4$. The flowfield was illuminated by the 532-nm light output of a frequency-doubled Nd:YAG laser. Water droplets and the $TiO_2$ particles were the only scatters in the flowfield, and they could be easily distinguished by their 50:1, or greater, diameter ratio. Water-droplet injection was controlled using a droplet-on-demand generator that was driven by a piezoelectric crystal transducer.[7]

Vortices form at roughly 20 Hz for the undriven shear layer, but they are not as stable as desired for the collection of phase-locked measurements and photographs. Therefore, vortex formation was controlled by acoustically driving the low-speed airstream at 20 Hz. A 1% velocity fluctuation was introduced into the low-speed side of the flow due to the acoustic driving. The natural shear layer and driven shear layer are very similar in appearance, but the vortices in the driven shear layer are more controlled and equally spaced. The location of the water droplets and the entrainment of the water vapor into the individual vortices of the shear layer, as marked by $TiO_2$ particles, were recorded with a digitizing camera. The curve identified by the location of the $TiO_2$ particles at the instant of visualization is referred to as a vaporline.

## Results and Discussion

A vaporline image of a two-dimensional shear layer in which a vortex is forming is shown in Fig. 1. The high-speed side of the flow is on the left and the low-speed side of the flow is on the right with flow from bottom to top. The left side of the flow is seeded with $TiCl_4$ vapor that reacts quickly and spontaneously with the water vapor from the droplets to form $TiO_2$ particles. Seven water droplets are visible in this particular image. The air on the left of the shear layer is moving faster than the droplets, and this causes the vapor to precede the droplets as they move downstream. Each droplet has a vaporline associated with it. More detailed analysis of images such as that shown in Fig. 1 led to the development of the schematic shown in Fig. 2 for describing the time and spatial development of the vaporlines.[5]

The vaporline schematic illustrates a specific case in which each droplet is introduced into a driven laminar flow at the same fre-

quency and phase angle (relative to the vortex generation) as the previous droplet. Therefore, this schematic provides an instantaneous picture of the flow that allows one to follow the development of vaporlines at a given flow phase angle, separated by 360-deg phase increments. The thick solid line represents a streakline that would form if dye or seed particles were emitted from the tip of the splitter plate. This streakline is shown to illustrate what the shear layer would look like using traditional methods. It is not created in the experimental shear layer unless a small droplet of water is placed on the tip of the splitter plate where it can react with $TiCl_4$ in the airflow to form $TiO_2$ particles. These particles would then be swept downstream from their origination site at the tip of the splitter plate. The dashed lines represent the particle trajectories that specific water droplets and $TiO_2$ particles would follow. The thin solid lines represent the vaporlines from each droplet. The open circles indicate the locations of the first $TiO_2$ seed particles formed when each water droplet first passed through the shear layer and to the $TiCl_4$-laden side of the flow. The same number is assigned to the head (water droplet) and the tail (first $TiO_2$ particle formed) of each vaporline. A continuous line of seed particles exists between each identically numbered droplet and seed particle. This line of seed (or vaporline) grows and stretches as it moves downstream, due to gaseous velocity gradients. It should be noted that the convective vaporline remains fairly thin and well defined over a long distance for the two-dimensional gaseous flows investigated, because these flows are laminar and well behaved. If the flow were turbulent, the vaporline would be a more disperse three-dimensional curve, and only a broken line might appear in a two-dimensional visualization.

Notice that the open-circle particles all lie on the streakline that originates at the tip of the splitter plate. It should not be assumed that as these individual seed particles move downstream, they remain on a path identical to the streakline shown. This would be the case only if the flow did not vary with time. However, since this flow is time-dependent, successive snapshots collected at other times (phase angles) would show the streaklines at different stages of their development. Furthermore, if the droplets are introduced at different times relative to the vortex generation, then the vaporlines will have slightly different shapes. This is because the droplets will see different surrounding airflows depending on where they are relative to the vortices. It would be easy to conclude that

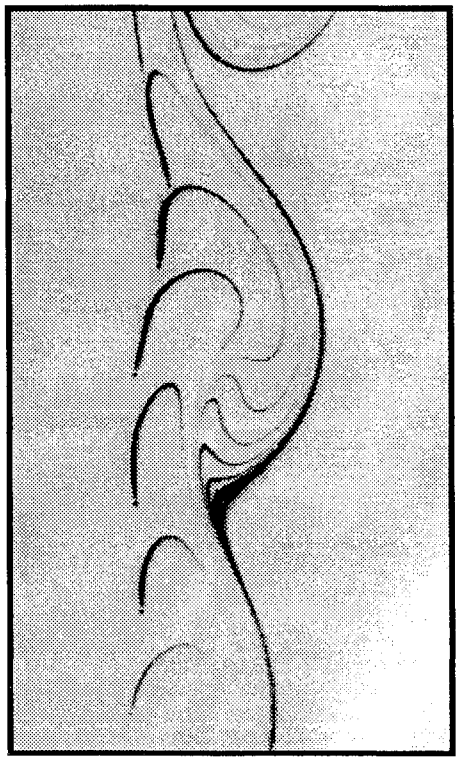

**Fig. 1 Vaporlines in a two-dimensional shear layer.**

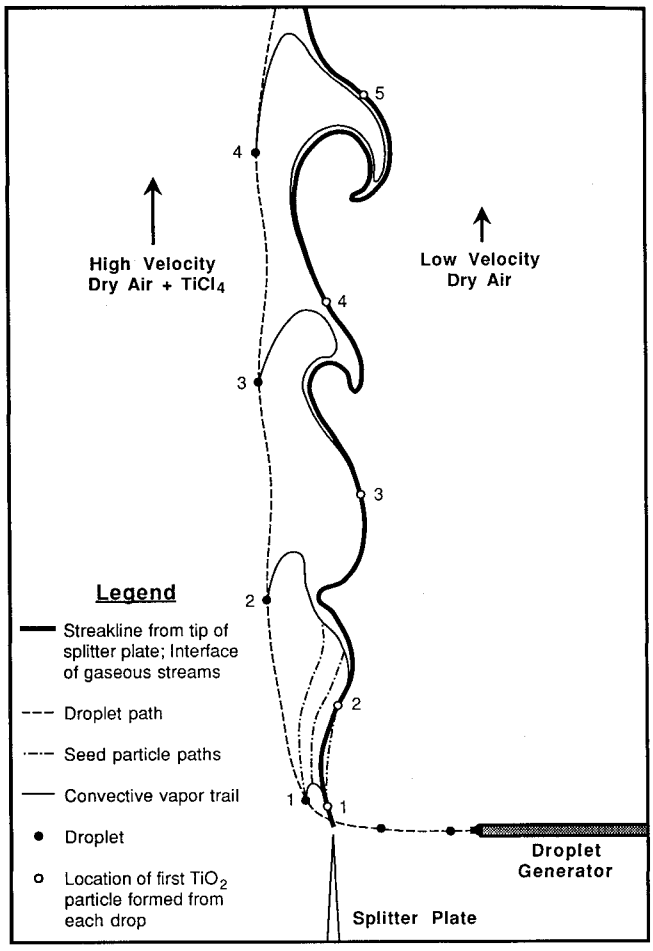


**Fig. 2 Vaporline schematic.**

the vapor from the droplets follows the path marked out by the vaporlines; this is not the case. The vaporlines are not streamlines or particle trajectories, but evolutionary histories of the convective vapor transport from a droplet relative to a specific flow. In this experiment no droplets, seed particles, or fluid elements move upstream, as observed from the laboratory reference frame. The fluid elements are moving downstream, but certain parts of the flow are moving faster than others, as reflected by the shape of the vaporline. The relative velocity of the droplet to the flow also plays a major role in defining the shape of the convective vaporline. In the extreme case, where the droplet is moving at the same velocity as the gas, no vaporline would exist—only a small spherical cloud of particles around the droplet where the evaporating water is reacting with the $TiCl_4$ would appear.

The vaporline visualization technique is fairly easy to use in low-velocity flows that are two-dimensional. However, if the flow is three-dimensional, this technique would be difficult using standard sheet-lighting techniques. Obviously, the $TiO_2$ vaporlines will form independent of the dimensionality of the flow or the method of flow illumination. However, in more turbulent flows the $TiO_2$ seed vaporlines will become more disperse, requiring a higher intensity light source to maintain sufficient light scattering for observation or recording. Furthermore, a nucleation time is associated with the growth of $TiO_2$ particles that are large enough to scatter sufficient light for observation. In the images shown in this Note, the time required for the $TiO_2$ particle to reach sufficient size for observation was ~2–3 ms. This could present a problem in high-velocity flows where the interesting fluid dynamics occurs over a time period much less than a few milliseconds.

With confidence that the basic fluid dynamics associated with these vaporlines was understood, attention was turned to the development of a numerical model to calculate vaporlines for comparison with experimental data. It was felt that if the vaporlines could

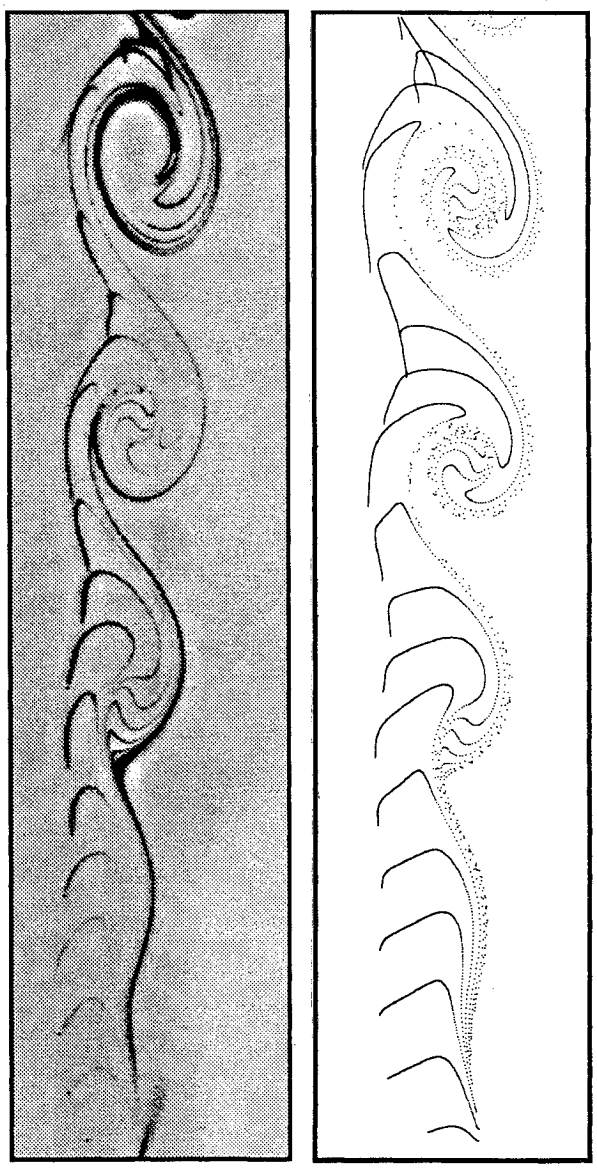

**Fig. 3 Vaporlines from tip of splitter plate for a two-dimensional shear layer (left: 0.70 m/s; right: 0.35 m/s; drive: 20 Hz; droplets: 100 Hz; and image: 3 × 12 cm).**

be modeled for a relatively simple two-dimensional flow, then it might be possible to extend this visualization technique to more complex flows such as boundary layers, jets in a crossflow, or other higher velocity flows.

The marker and cell (MAC) method was used to simulate the vaporlines of droplets in a two-dimensional shear layer. This numerical method was originally developed by Welch et al.[8] to solve flow systems with free surfaces. Later, it was modified by Hirt and Cook[9] to allow the pressure field to be solved more readily. The MAC method is characterized by the use of a staggered grid and the solution of the Poisson equation for pressure at every time step. Also, the pressure solution has the auxiliary task of satisfying the continuity condition. For visualization of the flow patterns (e.g., streaklines, vaporlines of droplets), massless markers (particles) convected by the velocity field were introduced. These markers play no role in determining the velocity and pressure fields.

Uniformly spaced MAC cells (0.1 × 0.05 cm) are distributed throughout the computational domain which is 30 cm long and 12.8 cm wide. The total number of cells is 300 × 256. To handle the outflow boundary condition, the "guard cells"[10] were used to extrapolate the velocity and pressure according to the following equations :

$$\left(\frac{\partial u}{\partial x}\right)_g = \left(\frac{\partial u}{\partial x}\right)_n \tag{1a}$$

$$P_g = P_n + (P_o - P_n)\left(\frac{X_g - X_n}{X_o - X_g}\right) \tag{1b}$$

where the subscript $g$ denotes the guard cell, and $n$ denotes the boundary cell. $X_g$ is the position of the guard cell relative to the origin. $X_n$ is the position of the boundary cell relative to the origin, and $X_o$ is the specified position of the ambient relative to the origin. In this program, artificial disturbances (1% and 20 Hz) were introduced along inflow boundaries to trigger the vortical-shedding process. The vaporlines of droplets observed in the experiments can be produced numerically by tracing a number of massless particles being emitted from the droplets while the droplets are traveling through the simulated flowfield. To obtain the particle velocities in the discretized flowfield numerically, an accurate second-order interpolation scheme from Chan et al.[11] was used.

The trajectories of droplets in the flowfield were calculated by employing the following drag correlation of droplets:[12]

$$C_D = \frac{3}{16} + \frac{24}{Re_d}, \qquad \text{for } Re_d \le 0.01 \tag{2a}$$

$$C_D = \frac{24}{Re_d}\{1 + 0.1315 Re_d^{[0.82 - 0.05\text{Log}_{10}(Re_d)]}\}$$

$$\text{for } 0.01 < Re_d \le 20 \tag{2b}$$

$$C_D = \frac{24}{Re_d}\{1 + 0.1935 Re_d^{0.6305}\}, \qquad \text{for } 20 < Re_d \le 260 \tag{2c}$$

The code was first used to predict the shape of the two-dimensional shear layer as marked by a streakline originating from the tip of the splitter plate. The experimental streakline was obtained by placing a small drop of water on the tip of the splitter plate and seeding the high-speed side of the flow with $TiCl_4$. The correlation between the experimental data and the model predictions is quite good. When droplets were introduced into the experimental shear layer, the image on the left in Fig. 3 was obtained. The resulting numerical simulation of this flowfield is shown on the right in the figure. The experimental data and the numerical results matched quite closely, despite limited information on the inlet velocity profile. Furthermore, the model does not account for a reduction in droplet diameter and weight due to evaporation. These droplets emit massless particles as they move in the flow to simulate the $TiO_2$ seed particle vaporlines formed when the water vapor comes in contact with the $TiCl_4$ in the flow.

## Conclusions

This Note describes a vaporline visualization technique and associated numerical model that are useful in characterizing the convective transport of vapor from evaporating droplets. The physical process has been modeled successfully, and the correlation between experimental data and model predictions is excellent. This visualization technique is easy to apply to low-velocity, two-dimensional flows, but its application becomes increasingly difficult in three-dimensional and high-velocity flows. However, it is anticipated that this visualization technique will be applied with some success to flows that are more complex than a two-dimensional shear layer.

## Acknowledgments

The authors acknowledge M. E. Post, V. R. Katta, D. Tankin, W. M. Roquemore, L. P. Goss, L. Brainard, D. D. Trump, and M. Whitaker for valuable insight and technical assistance. This work is supported by the Air Force Office of Scientific Research.

## References

[1]Melton, L. A., "Spectrally Separated Emissions for Diesel Fuel Droplets and Vapor," *Applied Optics*, Vol. 22, No. 14, 1983, pp. 2224–2226.

[2]Melton, L. A., and Verdieck, J. F., "Vapor/Liquid Visualization in Fuel

Sprays," *Twentieth Symposium (International) on Combustion*, Combustion Inst., Pittsburgh, PA, 1984, pp. 1283–1290.

[3]Ball, G. J., and Pratt, N. H., "Laser Induced Fluorescence Imaging of Interphase Mass Transfer in Steam/Water Flows," *Proceedings of the VI International Conference Photon Correlation and Other Techniques in Fluid Mechanics*, Inst. of Physics Conf. (Cambridge, England, UK), Serial 77, Session 3, 1985, pp. 111–116.

[4]Allen, M. G., and Hanson, R. K., "Digital Imaging of Species Concentration Fields in Spray Flames," *Twenty-First Symposium (International) on Combustion*, Combustion Inst., Pittsburgh, PA, 1986, pp. 1755–1761.

[5]Hancock, R. D., Jackson, T. A., and Nejad, A. S., "Technique for Visualizing Vaporlines Emanating from Water Droplets," *Applied Optics*, Vol. 31, No. 9, 1992, pp. 1163–1166.

[6]Chen, L.-D., and Roquemore, W. M., "Visualization of Jet Flames," *Combustion and Flame*, Vol. 66, No. 1, 1986, pp. 81–86.

[7]Switzer, G. L., "A Versatile System for Stable Generation of Uniform Droplets," *Review of Scientific Instruments*, Vol. 62, No. 11, 1991, pp. 2765–2771.

[8]Welch, J. E., Harlow, F. H., Shannon, J. P., and Daly, B. J., "The MAC Method, a Computing Technique for Solving Viscous, Incompressible Transient Fluid Involving Free Surface," Los Alamos Scientific Lab., Rept. LA-3425, Los Alamos, NM, 1966.

[9]Hirt, C. W., and Cook, J. L., "Calculating Three-Dimensional Flows Around Structures and Over Rough Terrain," *Journal of Computational Physics*, Vol. 10, No. 2, 1972, p. 324–340.

[10]Boris, J. P., Oran, E. S., Fritts, M. J., and Oswald, C. E., "Time Compressible Similarities of Shear Flows," Naval Research Lab., NRL Memo Rept. 5249, Washington, DC, 1983.

[11]Chan, R. K. C., Street, R. L., and Strelkoff, T., "Computer Studies of Finite Amplitude Water Waves," Stanford Univ., Dept. of Civil Engineering, TR 104, Stanford, CA, 1969.

[12]Clift, R., Grace, J. R., and Weber, M. E., *Bubbles, Drops, and Particles*, Academic Press, San Diego, CA, 1978, Chap. 5.

# Effect of Partial Thickness Actuation on Stress Concentration Reduction near a Hole

Pradeep K. Sensharma,* Mohammad H. Kadivar,† and Raphael T. Haftka‡
*Virginia Polytechnic Institute and State University, Blacksburg, Virginia 24061*

## Introduction

RECENTLY, there has been much interest in adaptive structures that can respond to a varying environment by changing their properties. Piezoelectric materials and shape memory alloys (SMA) are often used as partial thickness actuators to create such adaptivity by applied energy, usually electric current.[1,2] These actuators can be used to induce strains in a structure and reduce stresses in regions of high stress concentration.

Two of the present authors showed that axisymmetric actuation strains applied throughout the thickness of a plate with a hole can reduce the stress concentration factor (SCF) in an isotropic plate from 3 to 2 (Ref. 3). However, in most cases actuators are expected to be bonded to or embedded in the plate, so that the actuation strains are applied in the actuators and not directly in the plate.

The objective of this Note is to show that such partial-thickness actuation cannot be used to reduce the stress concentration factor with axisymmetric actuation strain distribution.

Received April 14, 1993; revision received Sept. 27, 1993; accepted for publication Sept. 27, 1993. 

*Graduate Research Assistant, Department of Aerospace and Ocean Engineering. Student Member AIAA.

†Visiting Professor, Shiraz University, Shiraz, Iran.

‡Christopher C. Kraft Professor, Department of Aerospace and Ocean Engineering. Associate Fellow AIAA.

## Problem Definition

A plate with a small hole under uniaxial tensile loading ($S$) with a ring of bonded and embedded actuators is shown in Fig. 1. The plate is treated analytically as an infinite plate. The radial, tangential, and shear-stress distribution for this case are given by[4]

$$\sigma_r^M = \frac{S}{2}\left[1-\left(\frac{A}{r}\right)^2\right]+\frac{S}{2}\left[1+3\left(\frac{A}{r}\right)^4-4\left(\frac{A}{r}\right)^2\right]\cos 2\theta \tag{1}$$

$$\sigma_\theta^M = \frac{S}{2}\left[1+\left(\frac{A}{r}\right)^2\right]-\frac{S}{2}\left[1+3\left(\frac{A}{r}\right)^4\right]\cos 2\theta \tag{2}$$

$$\tau_{r\theta}^M = -\frac{S}{2}\left[1-3\left(\frac{A}{r}\right)^4+2\left(\frac{A}{r}\right)^2\right]\sin 2\theta \tag{3}$$

where $A$ is the radius of the hole. In Ref. 3, our goal was to reduce the stress concentration as measured by Von-Mises or maximum shear-stress criteria by adding axisymmetric actuation strain fields with the piezoelectric actuators placed near the hole. The actuators account for only part of the thickness of the plate, being either bonded or embedded to the plate in the vicinity of the hole. Bonded and embedded actuators are shown in Fig. 1, where $t_a$ is the thickness of each actuator and $t_p$ is the thickness of the plate.

The total stresses at radius $r$ are given as

$$\sigma_r^{\text{tot}} = \sigma_r^M + \sigma_r^I, \quad \sigma_\theta^{\text{tot}} = \sigma_\theta^M + \sigma_\theta^I \tag{4}$$

where $\sigma_r^I$ and $\sigma_\theta^I$ are the radial and tangential stresses due to the actuator action, respectively. The Von-Mises equivalent stress is given by

$$\sigma_{\text{eq}} = \sigma_V = \sqrt{\sigma_1^2 - \sigma_1\sigma_2 + \sigma_2^2} \tag{5}$$

where $\sigma_1$ and $\sigma_2$ are the principal stresses calculated from the total stress components. The equivalent stress based on the maximum shear-stress criterion is given by

$$\sigma_{\text{eq}} = \sigma_{MS} = |\sigma_1 - \sigma_2| \tag{6}$$

when $\sigma_1$ and $\sigma_2$ are of the opposite sign. When $\sigma_1$ and $\sigma_2$ carry the same sign, then

$$\sigma_{\text{eq}} = \sigma_{MS} = \max(|\sigma_1|, |\sigma_2|) \tag{7}$$

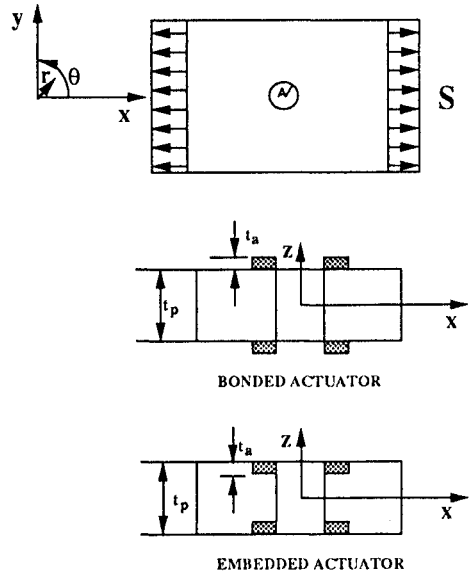


**Fig. 1 Bonded and embedded actuators near the hole.**